Applied Physics Letters

RESEARCH ARTICLE | JUNE 13 2023

Electronic transport mechanisms in a thin crystal of the Kitaev candidate α-$RuCl_3$ probed through guarded high impedance measurements

Patrick Barfield ; Vinh Tran ; Vikram Nagarajan ; Maya Martinez ; Amirari Diego ; Derek Bergner ; Alessandra Lanzara; James G. Analytis; Claudia Ojeda-Aristizabal

Appl. Phys. Lett. 122, 243102 (2023)
https://doi.org/10.1063/5.0146141

Applied Physics Letters ARTICLE pubs.aip.org/aip/apl

Electronic transport mechanisms in a thin crystal of the Kitaev candidate α-$RuCl_3$ probed through guarded high impedance measurements

Cite as: Appl. Phys. Lett. **122**, 243102 (2023); doi: 10.1063/5.0146141
Submitted: 10 February 2023 · Accepted: 30 May 2023 ·
Published Online: 13 June 2023

View Online Export Citation CrossMark

Patrick Barfield,[1] Vinh Tran,[1] Vikram Nagarajan,[2] Maya Martinez,[1] Amirari Diego,[1] Derek Bergner,[1] Alessandra Lanzara,[2,3] James G. Analytis,[2,3] and Claudia Ojeda-Aristizabal[1,a)]

AFFILIATIONS

[1]Department of Physics and Astronomy, California State University Long Beach, Long Beach, California 90840, USA
[2]Department of Physics, University of California Berkeley, Berkeley, California 94720, USA
[3]Materials Sciences Division, Lawrence Berkeley National Laboratory, Berkeley, California 94720, USA

[a)]Author to whom correspondence should be addressed: Claudia.Ojeda-Aristizabal@csulb.edu

ABSTRACT

α-$RuCl_3$ is considered to be the top candidate material for the experimental realization of the celebrated Kitaev model, where ground states are quantum spin liquids with interesting fractionalized excitations. It is, however, known that additional interactions beyond the Kitaev model trigger in α-$RuCl_3$ a long-range zigzag antiferromagnetic ground state. In this work, we investigate a nanoflake of α-$RuCl_3$ through guarded high impedance measurements aimed at reaching the regime where the system turns into a zigzag antiferromagnet. We investigated a variety of temperatures (1.45–175 K) and out-of-plane magnetic fields (up to 11 T), finding a clear signature of a structural phase transition at ≈160 K as reported for thin crystals of α-$RuCl_3$, as well as a thermally activated behavior at temperatures above ≈30 K, with a characteristic activation energy significantly smaller than the energy gap that we observe for α-$RuCl_3$ bulk crystals through our angle resolved photoemission spectroscopy (ARPES) experiments. Additionally, we found that below ≈30 K, transport is ruled by Efros–Shklovskii variable range hopping (VRH). Most importantly, our data show that below the magnetic ordering transition known for bulk α-$RuCl_3$ in the frame of the Kitaev–Heisenberg model (≈7 K), there is a clear deviation from VRH or thermal activation transport mechanisms. Our work demonstrates the possibility of reaching, through specialized high impedance measurements, the thrilling ground states predicted for α-$RuCl_3$ at low temperatures in the frame of the Kitaev–Heisenberg model and informs about the transport mechanisms in this material in a wide temperature range.

α-$RuCl_3$ is a van der Waals material predicted to host long-desired Kitaev quantum excitations, of interest for fault-tolerant topological quantum computing.[1–3] In α-$RuCl_3$, Ru^{3+} ions form a honeycomb lattice [Fig. 1(a)], where each ion is surrounded by an octahedral arrangement of Cl atoms. Neighboring octahedra are edge sharing, which according to the theoretical model by Jackeli and Khaliullin leads to dominant Kitaev interactions between spin–orbit entangled $j = 1/2$ moments of the Ru^{3+} ions, in contrast to corner sharing octahedra, which result in traditional symmetric Heisenberg interactions.[4] While honeycomb layers are bounded by van der Waals interactions, α-$RuCl_3$ has, at room temperature, a three-dimensional structure with a unit cell formed by three honeycomb layers stacked in an ABA configuration forming a rhombohedral crystal structure described by the $P3_112$ space group[5] (see the supplementary material). In the absence of crystal deformations, at low temperatures (below 155 K), the unit cell becomes monoclinic described by the C2/m space group[6] [see Fig. 1(b)]. In such a configuration, the system presents a 7 K transition to a magnetic order, where alternating chains of ferromagnets run along the zigzag direction of the honeycomb, referred to as a zigzag antiferromagnetic order, with the magnetic moments oriented ±35° from the ab plane.[6] It has been demonstrated that crystal deformations may lead to stacking faults and an additional, broader magnetic ordered transition at 14 K, attributed to a two-layer AB stacking order.[6]

Overall, the presence of a long-range magnetic order state in α-$RuCl_3$ derives from the existence of additional interactions beyond the Kitaev model. The true Hamiltonian for α-$RuCl_3$ is still controversial, but it is believed to be formed, in addition to a bond-dependent Kitaev ferromagnetic term ($K < 0$), of an isotropic Heisenberg term (J) that

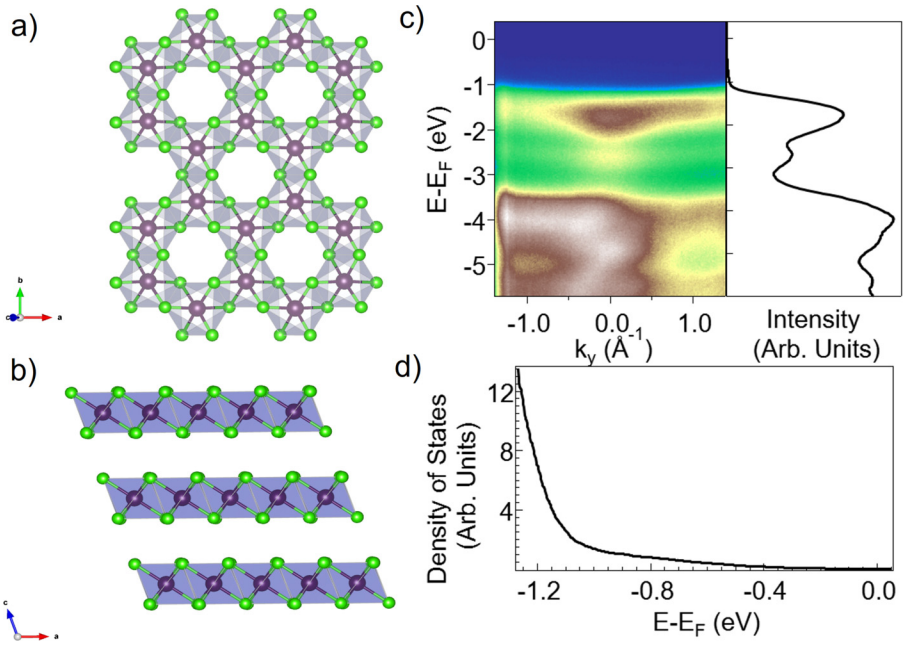

FIG. 1. Crystal and electronic structure of α-$RuCl_3$. (a) Crystal structure of α-$RuCl_3$, where Ru^{3+} ions form a honeycomb layer, with each ion surrounded by a Cl octahedral cage sharing an edge with its neighbors. (b) Low temperature C2/m arrangement of the honeycomb layers in an ABC configuration (see the text). (c) Measured electronic band structure in a k direction across Γ within the first Brillouin zone. Momentum integrated (in a range of $-1.0 \leq k_y \leq 1.0\,\text{Å}^{-1}$) energy distribution curve (EDC). (d) Spectral density of states deduced by dividing the momentum-integrated energy distribution curve (EDC) in (c) by a measured reference Fermi Dirac distribution, convoluted with a Gaussian that considers the instrument's energy resolution[7,8] (25 meV), showing that the density of states vanishes at the Fermi energy.

includes second and third order-neighbor interactions (the Kitaev–Heisenberg model), as well as of off diagonal antiferromagnetic Γ terms ($\Gamma > 0$) that are, like the Kitaev exchange, bond-directional. It has been demonstrated through resonant x-ray scattering[9] that the Γ term, which keeps the ordered momentum in the a-c plane,[10] is comparable to the Kitaev term K and is responsible for the observed large anisotropy of the magnetic susceptibility in α-$RuCl_3$.[11–14] The outcome of these multiple interactions in α-$RuCl_3$ is the previously mentioned zigzag antiferromagnetic ground state that can be conveniently suppressed by applying a ≈ 7 T in-plane magnetic field along the a direction [see Fig. 1(a)], yielding a quantum spin liquid (QSL)[15,16] and bringing experimentalists a step closer to the desired anyonic excitations predicted in the frame of the Kitaev model.[17] Much stronger fields are needed in the c direction (up to ≈ 33 T) to destroy the zigzag antiferromagnetic order and reach a quantum spin liquid state, as recently reported.[18]

From an electronic point of view, α-$RuCl_3$ is a transition metal oxide with partially filled 4d shells (a halide). Despite the expected large atomic overlap that should lead to large electronic bandwidths and a metallic behavior, important spin–orbit coupling triggers the formation of separate $j = 3/2$ and $j = 1/2$ bands, leading, regardless of largely suppressed electronic correlations, to a Mott insulating state.[1,19]

Here, we study through electronic transport measurements at low temperatures an α-$RuCl_3$ thin crystal device, finding the different electronic transport mechanisms that rule this Kitaev candidate material in a wide range of temperatures. In particular, we find evidence of a deviation from a Efros–Shklovskii variable range hopping (ES-VRH) transport mechanism at temperatures below the zigzag antiferromagnetic order transition explained in the frame of the Kitaev–Heisenberg model.

Sample fabrication was performed as indicated in the supplementary material. Finished devices shown in Figs. 2(a) and 2(b) were mounted to a custom triax probe [Fig. 2(d)] to be later measured in a closed-cycle cryostat. The use of triax lines allows for guarded measurements to improve the signal to noise ratio as experiments are performed at low temperatures where α-$RuCl_3$ crystals are highly insulating. As the sample resistance at low temperatures is comparable to the insulation of the lines, leakage currents have the potential to corrupt the signal from the sample. In a guarded configuration, the inner core and inside shield of the triax lines are connected to the ammeter terminals that result in negligible leak currents [see Fig. 2(c) and supplementary material for details]. Additionally, the guard terminal of the instrument is connected to a copper sample enclosure [shown in Fig. 2(d)], which serves to further isolate the sample from electromagnetic interference, where any current noise generated by surrounding AC or DC fields or coupling capacitances is kept away from the sample [see Fig. 2(e)].

Current–voltage (I–V) characteristics of the α-$RuCl_3$ device were measured using the triax probe and an electrometer (Keithley 6517B), across a temperature range from 1.45 to 130 K as shown in Figs. 3(a) and 3(b), and in the presence of out-of-plane magnetic fields up to 11 T. Current values at fixed biases were taken from each curve and fit to different transport mechanisms dependent on the temperature and bias voltage regime as outlined in Fig. 3(c). The electrodes used in this measurement are the top two depicted in Fig. 2(b) with edge width of 1.0 μm and spacing from 1 μm at the widest to 200 nm at the narrowest.

Overall, the measured I–V curves showed an ohmic behavior at 130 K with increasing non-linearity and decreasing slope as the temperature is lowered, reaffirming the Mott insulating character of the material[1,20] as represented in Figs. 3(a) and 3(b). We then represented the data in an appropriate semi-log scale in accordance with the regimes presented in Fig. 3(c). In particular, we found that for low bias voltage and low temperatures, the data best support temperature dependent Efros–Shklovskii variable range hopping. At low bias and

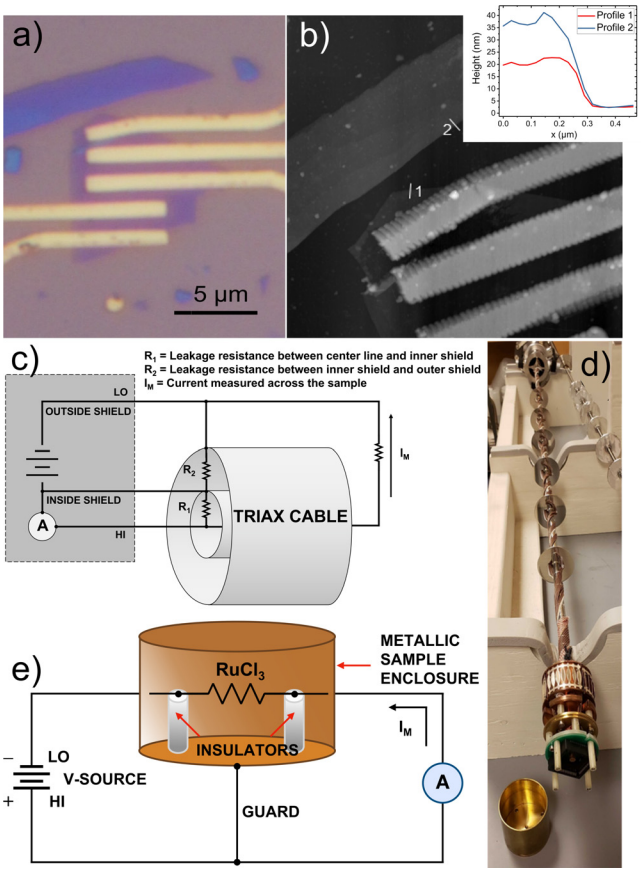

FIG. 2. Fabricated device and experimental setup. 100× optical (a) and atomic force microscopy (AFM) (b) images of the completed α-$RuCl_3$ device. The inset shows the measured height of α-$RuCl_3$ nanoflake used for the device alongside a nearby, thicker nanoflake for comparison. (c) Circuit schematic of the guarded force-voltage-measure-current setup used in this experiment making use of triax lines, wired to a custom probe with a copper sample enclosure (d). (e) Schematic showing the connection of the guard to the sample enclosure.

high temperatures, thermal activation dominates, while for high bias, transport is field-assisted as shown in Fig. 3.

At higher temperatures (30–130 K) and low bias (25 mV), we observe that transport is thermally activated and fits to an Arrhenius law. That is, the current I has a dependence on the temperature of the following form:

$$I \propto \exp\left(\frac{-E_A}{k_B T}\right), \tag{1}$$

where E_A is the activation energy, and k_B is Boltzmann's constant. By fitting the data to Eq. (1) [Fig. 4(d)], we extract an activation energy $E_A \approx 9$meV at 25 mV bias voltage that decreases with increasing bias voltage, because the carrier activation is facilitated by the increasing in-plane electric field. As a consequence, as observed in Fig. 4(d), the temperature range in which the data fits thermal activation shrinks at higher bias voltages.

The activation energy that we deduce, E_A, is several orders of magnitude smaller than the energy bandgap, which we observed through angle-resolved photoemission spectroscopy (ARPES) for bulk crystals of α-$RuCl_3$ (at least 1.2 eV) and reported in the literature.[20,21] We attribute this to impurity states induced in the gap via charge trapping in the SiO_2 substrate, as has been found for atomically thin semiconductors, such as MoS_2.[22] Due to the size of the gap, fluctuations in the trapped charges at the interface between the crystal and the substrate should not be effectively screened at lower temperatures.[23,24] In this temperature range (30–130 K), where the temperature is much smaller than the known energy gap for α-$RuCl_3$, we believe that carriers hop between nearest neighbor electron and hole-doped areas.

At low temperatures and low bias, conduction tends to be more appropriately described by a variable range hopping (VRH) law,

$$I \propto \exp\left(-\left(\frac{T_0}{T}\right)^{\nu}\right), \tag{2}$$

where T_0 is the characteristic temperature whose energy scale is related to the localization length of the charge carriers. Taking $\nu = 1/3$ and $\nu = 1/4$ gives Mott's VRH law for 2D and 3D hopping conduction, respectively. Mott's VRH law describes hopping of carriers between remote sites in a narrow band near the Fermi level.[25] Bulk α-$RuCl_3$ has a 1.2–1.9 eV Mott insulating gap with a zero density of states near the Fermi level as reported in the literature[20,21] and corroborated with our ARPES measurements [Figs. 1(c) and 1(d)], which disfavors Mott VRH as a possible transport mechanism for bulk α-$RuCl_3$. However, we believe that in our thin crystal device, the presence of molecules from air trapped between the α-$RuCl_3$ and the SiO_2 substrate creates a narrow band of localized states near the Fermi level, facilitated by α-$RuCl_3$'s large work function ($\Phi_{RuCl_3} = 6.1$ eV[26,27]) Furthermore, we believe that electronic correlations between these impurities create a soft Coulomb gap in the density of states, as developed in the following.

In the presence of Coulomb correlations, the Miller–Abrahams random resistor network model that guides the theory of VRH conduction is no longer appropriate. In this regime, transport is described by Efros and Shklovskii's $\nu = 1/2$ variable range hopping (ES-VRH), that reformulates the random resistor network model in the presence of electronic correlations.[23,28] In that case, the current across the device is given by

$$I \propto \exp\left(-\left(\frac{T_0}{T}\right)^{1/2}\right), \quad T_0 = \frac{2.8e^2}{4\pi\varepsilon\varepsilon_0 k_B a}, \tag{3}$$

where e is the electron charge, ε is the dielectric constant of the material, ε_0 is the permittivity of free space, and a is the localization length of the charged impurities.

Indeed, by comparing the fitting of our low temperature data between 3D Mott variable range hopping and ES-VRH models, we find that the latter is better suited, as shown in Fig. S1 in the supplementary material. Most importantly, we estimate the Coulomb gap Δ created by the charged impurities at the α-$RuCl_3$ thin crystal—substrate interface within the ES-VRH theory,[23] which gives the gap width $\Delta = e^3 g_0^{1/2}/(4\pi\varepsilon\varepsilon_0)^{3/2} \sim 4.5$ meV, where $\varepsilon \sim 7.4$ for α-$RuCl_3$[29] and $g_0 \sim 2.2 \times 10^{19}$ $eV^{-1}cm^{-3}$ is the unperturbed density of states of the charged impurities, estimated from the typical density of charge traps at the SiO_2 interface 4×10^{12} $eV^{-1}cm^{-2}$ (Refs. 22, 30, and 31) over our 18 nm thick crystal. This estimation of the Coulomb gap places us at low temperatures in a regime where $\Delta \gg k_B T$. Also,

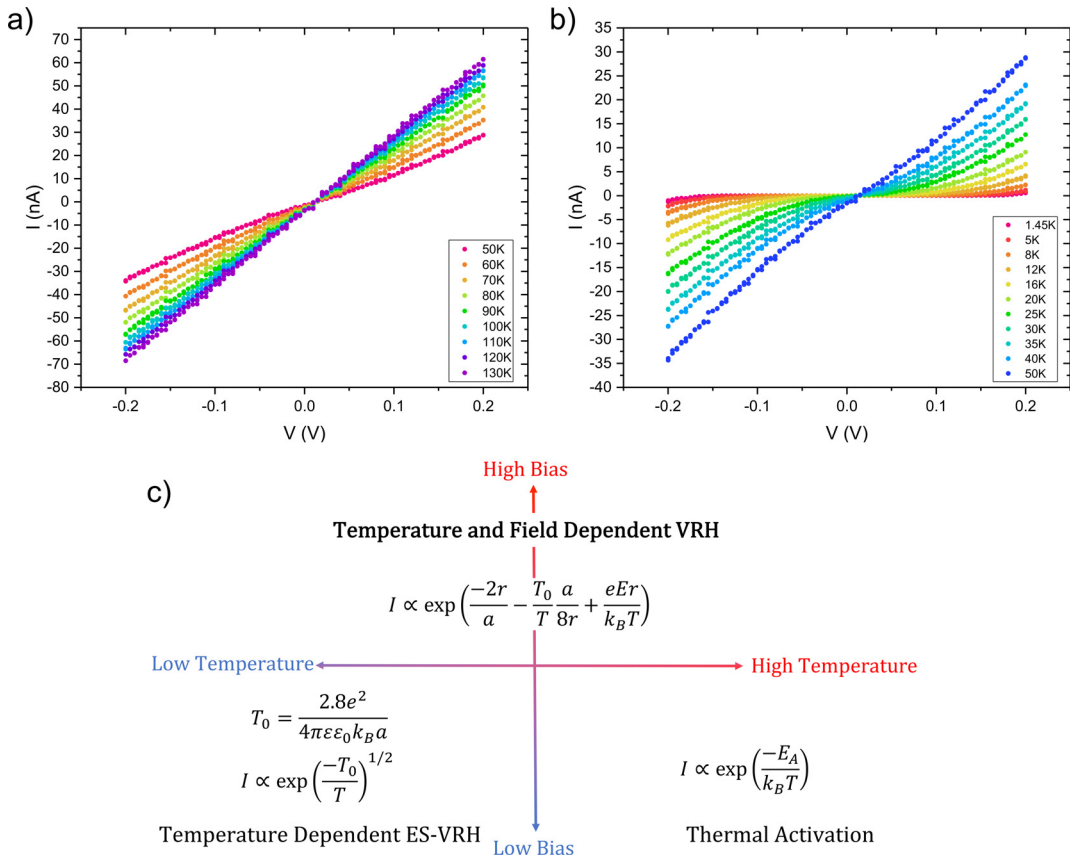

FIG. 3. I–V dependence and transport mechanisms in different regimes. Current–voltage characteristics for α-$RuCl_3$ device showing a (a) linear, ohmic behavior at high temperatures and a (b) nonlinear behavior at low temperatures. The decreasing slope of the curves with decreasing temperatures is characteristic of a highly insulating behavior. (c) Schematics of the dominant transport mechanisms at the different regimes. Low temperatures (<30 K) and low bias (25 mV) are ruled by Efros–Shklovskii variable range hopping (bottom-left quadrant), high temperatures, and low bias by a thermal activation mechanism (bottom-right quadrant), while high bias is dominated by an electric field-assisted hopping (top-right and top-left quadrants).

the value we find for the Coulomb gap $\Delta \sim 4.5$ eV is similar to activation energy deduced in the high temperature and low bias regime (detailed above).

By plotting the log of the current as a function of $T^{-1/2}$, we find that ES-VRH fits well our data at low temperatures and low biases. For the lowest bias voltage used (25 mV), we observe that the ES-VRH mechanism rules the electronic transport in our sample down to the zigzag antiferromagnetic ordering transition at ∼7 K (predicted in the frame of the Heisenberg–Kitaev model) as shown in Fig. 4(c), in a temperature range where $\Delta \gg k_B T$ (7–40 K).

From our semi-log plot, a linear fit of the data allows us to extract T_0 deducing a localization length $a \approx 3$ nm [Eq. (3)]. This is a similar value to the one we deduced in the past for another spin–orbit assisted Mott insulator (Na_2IrO_3),[32] where variable range hopping is mediated by a quasiparticle at the Fermi level that results from the Ir–O octahedra embedded between two Na layers creating a charge transfer from Na to Ir in Na_2IrO_3.[32,33] Additionally, VRH has been reported in thin crystals of α-$RuCl_3$.[34] Although the origin of a non-zero density of states at the Fermi level is not commented in Ref. 34, it may have the same origin as in our samples, charged impurities from the SiO_2 substrate. Transport data in that work may also be fitted to ES-VRH, yielding similar characteristic energies to those in our samples.

At high bias voltages (up to 0.2 V), the energy difference in hopping sites is compensated by the electric field. Following Shklovskii's theory of hopping conduction in the presence of a strong electric field,[35] we use an engineered expression for intermediate fields introduced in Ref. 36,

$$I \propto \exp\left(-\frac{2r}{a} - \frac{T_0}{T}\frac{a}{8r} + \frac{erE}{k_B T}\right). \quad (4)$$

Here, the Miller and Abrahams relation for hopping conduction[23] is modified to include the contribution from the field, leading for $E = 0$ to the ES-VRH expression [Eq. (2)]. On the other hand, when the electric field exceeds a critical value, $E_C \approx \frac{2k_B T}{ea}$, the energy required for hopping is fully compensated by the field. As a result, the second and third terms in expression (4) cancel each other out (see the supplementary material), leading to a temperature independent transport mechanism,[36] consistent with Shklovskii's theory,[35]

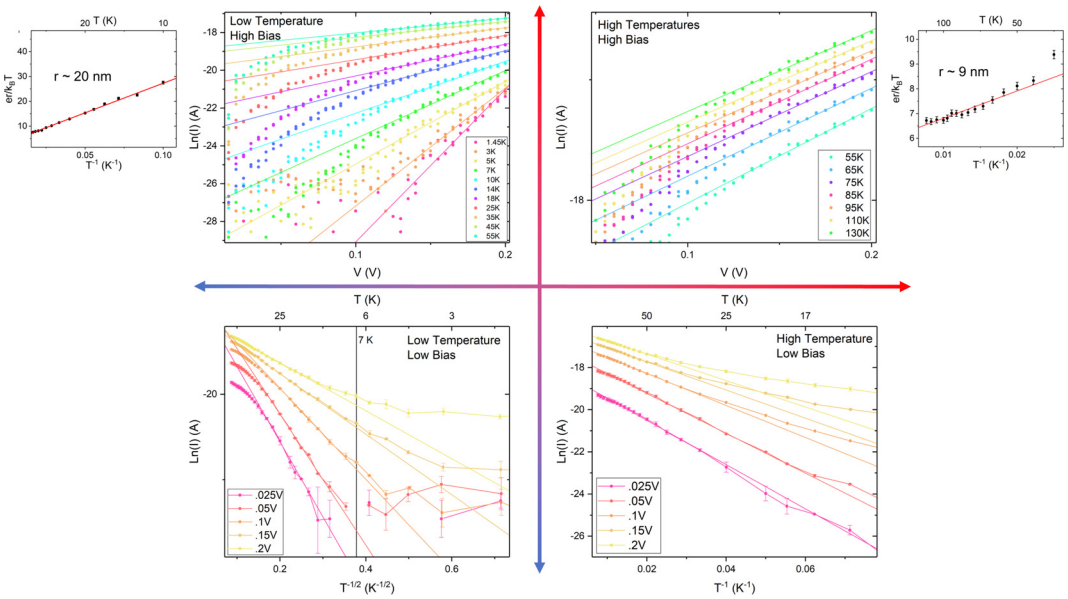

FIG. 4. Electronic transport mechanisms in four different regimes. A schematic that depicts four different regimes segmented by temperature and bias, where data are represented as a semi-log plot of ln (I) in accordance with the transport mechanism dominant in that regime, according to Fig. 3(c). In (a) and (b), for high V and low and high T, respectively, conduction is dominated by field assisted ES-VRH. Insets show the mean hopping length, r, deduced from the linear fits shown in (a) and (b). Instead for low T and low V, temperature dependent ES-VRH instead fits best (c). For high T and low V (d), a thermally activated nearest-neighbor hopping mechanism is more prevalent.

$$I \propto \exp\left(-\left(\frac{E_0}{E}\right)^{1/2}\right), \quad E_0 = \frac{k_B T_0}{2ea}. \tag{5}$$

Indeed, Eq. (4) is in reasonable agreement with numerical results reported for fields below E_C.[37] Using the previously found value for the localization length $a \approx 3$ nm, we estimate the critical field to be $E_C > 0.2\,\mathrm{V}/\mu\mathrm{m}$ for temperatures above the 7 K magnetic ordering transition. As our range of fields here are 0.0–0.2V/μm, transport in this regime is not fully driven by the electric field and is dependent on both the temperature and the field, following, therefore, Eq. (4). A semi-log plot of I vs V allows us to extract the temperature dependence of the third term in Eq. (4) by fitting each of our I–V curves [see Fig. 4(a)]. By analyzing this temperature dependence, we acquire the mean hopping length, r [see insets of Figs. 4(a) and 4(b)]. In a temperature range from 130 to 55 K, we calculate $r \approx 9$ nm, while in a lower range of temperatures of 55 to 10 K, r is instead ≈ 20 nm. We observe, therefore, a shorter hopping distance at higher temperatures, indicating that as temperature increases, carriers are more likely to hop to spatially neighboring sites. A longer hopping length at lower temperatures is consistent with variable range hopping mechanisms as carriers look to more distant sites to find energetically favorable hops. Such behavior can be seen directly in the data, in the temperature dependence of the slopes of the fitted data in Figs. 4(a) and 4(b) (field-assisted regime). Above a temperature of ≈ 55 K [Fig. 4(b)], the slopes change very little with the temperature, indicating that the activation energy is compensated less by the field and that shorter hops are favored. As temperature decreases [Fig. 4(a)], the slopes increase, and hops cover in average more distance, in the direction of the electric field.

Our data show that while electronic transport in a thin crystal of α-$RuCl_3$ can be well understood in a wide range of temperatures, it goes beyond ES-VRH or thermal activation below the magnetic ordering transition at 7 K. This result is in line with our previous work on the spin–orbit assisted insulator Na_2IrO_3.[32]

We noted no change in the transport mechanism near 14 K, where a magnetic ordering transition has been reported for α-$RuCl_3$ crystals with a two-layer AB stacking order (instead of a ABC configuration). This points to a α-$RuCl_3$ thin crystal device free of deformations or stacking faults.[6]

We observed no change in any of the transport mechanisms in the thin flake of α-$RuCl_3$ or the deduced transport quantities, when an out-of-plane magnetic field up to 11 T was applied, as seen in Fig. 5. This is consistent with the known magnetic anisotropy in α-$RuCl_3$, that as mentioned in the introduction, results in a critical field that increases dramatically from the in-plane (≈ 7 T) to the out-of-plane direction (≈ 33 T).[14,18]

Finally, we want to point out that in a second α-$RuCl_3$ thin crystal sample, where I–V curves were measured up to 175 K, we observed a drastic change in the conductance at $\approx$160 K by almost three orders of magnitude, apparent in both cooling down and warming up cycles (see Fig. 6). We believe that this is the signature of the structural phase transition from space group $P3_112$ at high temperatures to space group C2/m below $\approx$160 K, reported through neutron diffraction experiments for exfoliated thin crystals of α-$RuCl_3$,[5] and puts in evidence the reliability of our high impedance guarded measurements. While the major difference between the $P3_112$ and C2/m structures is the c-ordering of the Ru honeycomb layers (see the supplementary material), there are also differences within each honeycomb layer that have important implications in the electronic structure. α-$RuCl_3$'s trigonal high temperature structure $P3_112$ has shorter Ru–Ru bonds, and, therefore, Ru–Ru hopping dominates in this structure.[12] On the other

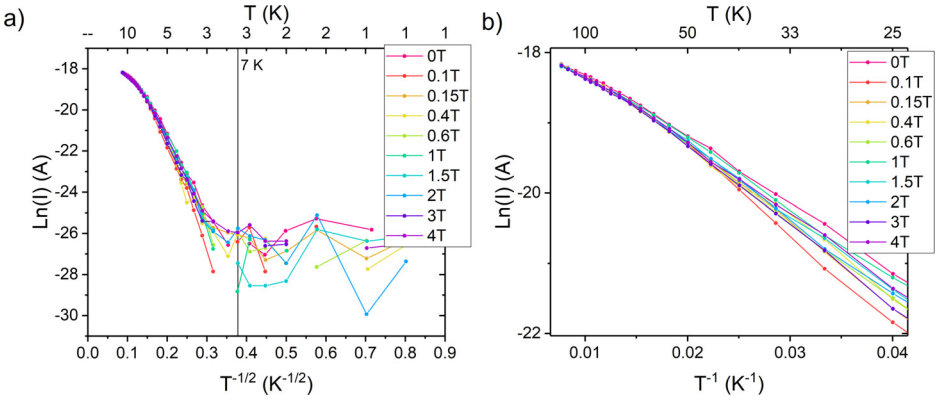

FIG. 5. Effect of an out-of-plane magnetic field on the transport mechanisms. Data taken from I–V curves at 50 mV in a range of magnetic fields perpendicular to the honeycomb lattice, from 0 to 4 T plotted as ln (I) vs $T^{-1/2}$ in fitting to Efros–Shklovskii variable range hopping (a) and as ln (I) vs T^{-1} in fitting to thermal activation (b). We do not see a consistent effect of an out-of-plane magnetic field on the transport, either above or below the magnetic ordering transition (7 K).

hand, in the monoclinic low temperature structure C2/m, the dominant hopping process occurs via Cl states creating quasimolecular orbitals (QMOs) made of a linear combination of the t_{2g} states of the six Ru atoms in each hexagon.[38–40] In that case, every electron is localized within the six crystal sites of α-$RuCl_3$ that form a hexagon, mimicking a molecular orbital. This important difference between the two crystal structures (Ru–Ru hopping vs localized molecular orbitals centered on each hexagon) can explain the sudden drop in current across the structural phase transition. The shift in the curve cooling down vs warming up [inset of Fig. (6)], where the sample converges to a different resistance value in the low temperature C2/m structure, is possibly related to a slightly different stacking of the α-$RuCl_3$ layers that may impact the electron hopping mechanism.

In summary, we fabricated an electronic device of a mechanically exfoliated α-$RuCl_3$ nanoflake. The use of guarding and triax lines allowed us to isolate the high impedance input of our measuring instrument (an electrometer) from leakage currents in the experimental setup, granting us access to electronic transport measurements in our α-$RuCl_3$ devices at temperatures as low as 1.5 K. Additionally, the use of a custom-made metallic shielding around our sample allowed us to reduce the noise associated with electrostatic interference. With the help of these techniques, we found that at low bias voltages, transport is thermally activated at high temperatures (30–130 K) and follows Efros–Shklovskii (ES) variable range hopping at low temperatures (≈7–30 K). With increasing bias, the transport mechanism changes to a field-assisted one, but it is not entirely field driven within the voltage range used in this experiment. From these different models, we deduced the presence of charged impurities, possibly originating at the SiO_2/α-$RuCl_3$-thin crystal interface, with a localization length of $a \approx 3$nm. We observed mean hopping lengths at different temperature ranges in the field-assisted regime, following the expected behavior for variable range hopping at lower temperatures, where charge carriers hop to remote sites with close energy levels. Most importantly, we found that ES-VRH is suppressed below the zigzag antiferromagnetic ordering transition temperature known for bulk α-$RuCl_3$, 7 K, and is consistent with the Kitaev–Heisenberg model. This behavior is unaffected by the presence of magnetic fields in the c-axis (perpendicular to the honeycomb plane) as large as 11 T, agreeing with recent results that suggest the suppression of the magnetic ordered state in α-$RuCl_3$ only at out-of-plane fields larger than 33 T.[18] Finally, we observed the signature of the structural phase transition reported for thin crystals of α-$RuCl_3$,[5] which testifies the fidelity of our technique at measuring high impedance samples. Future experiments will take advantage of the strong magnetic anisotropy in α-$RuCl_3$, using an in-plane magnetic field, for which the critical field is considerably reduced.[15,16] In the presence of such a field, we expect the long range magnetic order to disappear, and similar experiments as those reported here would likely show a deviation from standard transport mechanisms such as variable range hopping or thermal activation at temperatures at which the system transitions from a conventional paramagnet into a spin liquid, although this is currently ill-defined in the literature.

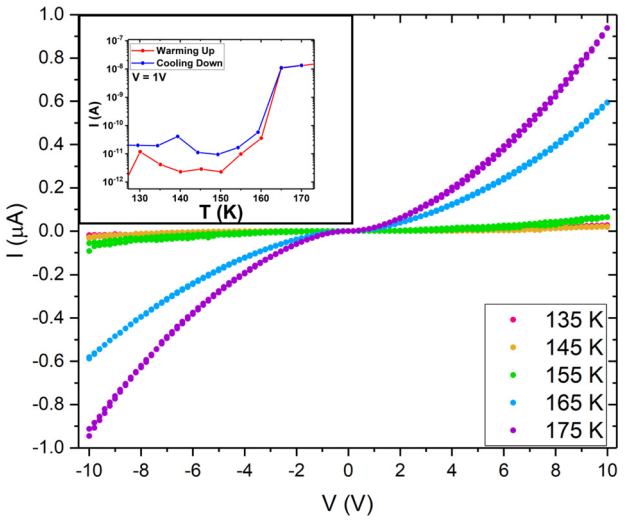

FIG. 6. Signature of structural phase transition in a thin crystal of α-$RuCl_3$. I–V characteristics of a separate thin crystal device of α-$RuCl_3$, measured up to 175 K, where a striking change in the conductance of the sample at 160 K can be observed, best seen in the inset, where the current from I–V curves at different temperatures was extracted at bias voltage 1 V.

See the supplementary material for details on the sample preparation and measurements; a comparison of the room temperature and low temperature unit cells of α-$RuCl_3$; a figure comparing the fits of Efros–Shklovskii variable range hopping vs 3D Mott variable range

hopping in the low temperature and low bias regime (Fig. S1); and calculations demonstrating that the expression describing transport mechanisms in intermediate regimes, Eq. (4), reduces to temperature dependent ES-VRH hopping $\sim \exp\left(-(T_0/T)^{1/2}\right)$ [Eq. (3)] in the limit of low temperatures and low fields and to field assisted ES-VRH hopping in the limit of strong fields $\sim \exp\left(-(E_0/E)^{1/2}\right)$ [Eq. (5)].

The primary funding for this work was provided by the U.S. Department of Energy, Office of Science, Office of Basic Energy Sciences under Contract No. DE-SC0018154. D.B. was supported for ARPES data analysis by the Cal. State. Long Beach and Ohio State University Partnership for Education and Research in Hard and Soft Materials, a National Science Foundation PREM, under Grant No. 2122199. The crystal growth work by V.N. and J.G.A. was supported by the National Science Foundation under Grant No. 1905397. Atomic force microscopy imaging was supported by the National Science Foundation, MRI program, under Award No. NSF-MRI 2018653. The photoemission work by A.L. was supported by the U.S. Department of Energy, Office of Science, Office of Basic Energy Sciences, Materials Sciences and Engineering Division, under Contract No. DE-AC02-05CH11231 within the vdW heterostructure Program (KCWF16). The Advanced Light Source was supported by the Director, Office of Science, Office of Basic Energy Sciences, of the U.S. Department of Energy (U.S. DOE-BES) under Contract No. DE-AC02-05CH11231. We would like to acknowledge invaluable advice from Professor Boris Shklovskii regarding our theoretical treatment of intermediate regimes, as well as Jonathan Denlinger from the Advanced Light Source at LBL for advice on ARPES measurements, David Warren from Oxford Instruments for crucial guidance on our triax lines probe, and Nicholas Breznay for advice on high impedance measurements. P.B. would like to acknowledge the Margaret Heeb Summer Research Assistantship in Honor of Wilma Jordan Olaf and the Mary Jane Anfinson Endowed Scholarship at CSULB. P.B. and V.T. would like to acknowledge the Richard D. Green Graduate Research Fellowship from the College of Natural Sciences and Mathematics at CSULB. M.M would like to acknowledge the Google American Physical Society Inclusive Graduate Education Network Bridge Fellowship Program at CSULB.

AUTHOR DECLARATIONS

Conflict of Interest

The authors have no conflicts to disclose.

Author Contributions

Patrick Barfield: Conceptualization (equal); Data curation (equal); Formal analysis (equal); Investigation (equal); Methodology (equal); Writing – original draft (lead). **Vinh Tran:** Conceptualization (equal); Data curation (equal); Formal analysis (equal); Investigation (equal); Writing – original draft (lead). **Vikram Nagarajan:** Investigation (equal). **Maya Martinez:** Conceptualization (equal); Data curation (equal); Investigation (equal). **Amirari Diego:** Conceptualization (supporting); Data curation (supporting); Investigation (supporting). **Derek Bergner:** Data curation (supporting); Formal analysis (supporting). **Alessandra Lanzara:** Conceptualization (supporting); Funding acquisition (supporting); Investigation (equal). **James Analytis:** Conceptualization (supporting); Funding acquisition (supporting); Investigation (equal). **Claudia Ojeda-Aristizabal:** Conceptualization (lead); Data curation (equal); Formal analysis (equal); Funding acquisition (lead); Investigation (lead); Methodology (equal); Project administration (lead); Supervision (lead); Validation (lead); Writing – review & editing (lead).

DATA AVAILABILITY

The data that support the findings of this study are available from the corresponding author upon reasonable request.

REFERENCES

[1]K. W. Plumb, J. P. Clancy, L. J. Sandilands, V. V. Shankar, Y. F. Hu, K. S. Burch, H.-Y. Kee, and Y.-J. Kim, "α-$RuCl_3$: A spin-orbit assisted Mott insulator on a honeycomb lattice," Phys. Rev. B **90**, 041112 (2014).
[2]H.-S. Kim, S. Vijay Shankar, A. Catuneanu, and H.-Y. Kee, "Kitaev magnetism in honeycomb $RuCl_3$ with intermediate spin-orbit coupling," Phys. Rev. B **91**, 241110 (2015).
[3]H. Takagi, T. Takayama, G. Jackeli, G. Khaliullin, and S. E. Nagler, "Concept and realization of Kitaev quantum spin liquids," Nat. Rev. Phys. **1**, 264 (2019).
[4]G. Jackeli and G. Khaliullin, "Mott insulators in the strong spin-orbit coupling limit: From Heisenberg to a quantum compass and Kitaev models," Phys. Rev. Lett. **102**, 017205 (2009).
[5]M. Ziatdinov, A. Banerjee, A. Maksov, T. Berlijn, W. Zhou, H. B. Cao, J.-Q. Yan, C. A. Bridges, D. G. Mandrus, S. E. Nagler, A. P. Baddorf, and S. V. Kalinin, "Atomic-scale observation of structural and electronic orders in the layered compound α-$RuCl_3$," Nat. Commun. **7**, 13774 (2016).
[6]H. B. Cao, A. Banerjee, J.-Q. Yan, C. A. Bridges, M. D. Lumsden, D. G. Mandrus, D. A. Tennant, B. C. Chakoumakos, and S. E. Nagler, "Low-temperature crystal and magnetic structure of α-$RuCl_3$," Phys. Rev. B **93**, 134423 (2016).
[7]T. Sato, T. Yokoya, Y. Naitoh, T. Takahashi, K. Yamada, and Y. Endoh, "Pseudogap of optimally doped $La_{1.85}Sr_{0.15}CuO_4$ observed by ultrahigh-resolution photoemission spectroscopy," Phys. Rev. Lett. **83**, 2254–2257 (1999).
[8]T. Susaki, Y. Takeda, M. Arita, K. Mamiya, A. Fujimori, K. Shimada, H. Namatame, M. Taniguchi, N. Shimizu, F. Iga, and T. Takabatake, "Temperature-dependent high-resolution photoemission study of the Kondo insulator YbB_{12}," Phys. Rev. Lett. **82**, 992–995 (1999).
[9]J. A. Sears, L. E. Chern, S. Kim, P. J. Bereciartua, S. Francoual, Y. B. Kim, and Y.-J. Kim, "Ferromagnetic Kitaev interaction and the origin of large magnetic anisotropy in α-$RuCl_3$," Nat. Phys. **16**, 837 (2020).
[10]J. C. V. Chaloupka and G. Khaliullin, "Magnetic anisotropy in the Kitaev model systems Na_2IrO_3 and $RuCl_3$," Phys. Rev. B **94**, 064435 (2016).
[11]J. A. Sears, M. Songvilay, K. W. Plumb, J. P. Clancy, Y. Qiu, Y. Zhao, D. Parshall, and Y.-J. Kim, "Magnetic order in α-$RuCl_3$: A honeycomb-lattice quantum magnet with strong spin-orbit coupling," Phys. Rev. B **91**, 144420 (2015).
[12]R. D. Johnson, S. C. Williams, A. A. Haghighirad, J. Singleton, V. Zapf, P. Manuel, I. I. Mazin, Y. Li, H. O. Jeschke, R. Valentí, and R. Coldea, "Monoclinic crystal structure of α-$RuCl_3$ and the zigzag antiferromagnetic ground state," Phys. Rev. B **92**, 235119 (2015).
[13]Y. Kubota, H. Tanaka, T. Ono, Y. Narumi, and K. Kindo, "Successive magnetic phase transitions in α-$RuCl_3$: XY-like frustrated magnet on the honeycomb lattice," Phys. Rev. B **91**, 094422 (2015).
[14]M. Majumder, M. Schmidt, H. Rosner, A. A. Tsirlin, H. Yasuoka, and M. Baenitz, "Anisotropic ru^{3+} $4d^5$ magnetism in the α-$RuCl_3$ honeycomb system: Susceptibility, specific heat, and zero-field NMR," Phys. Rev. B **91**, 180401 (2015).
[15]Y. Kasahara, T. Ohnishi, Y. Mizukami, O. Tanaka, S. Ma, K. Sugii, N. Kurita, H. Tanaka, J. Nasu, Y. Motome, T. Shibauchi, and Y. Matsuda, "Majorana quantization and half-integer thermal quantum Hall effect in a Kitaev spin liquid," Nature **559**, 227 (2018).

[16]P. Czajka, T. Gao, M. Hirschberger, P. Lampen-Kelley, A. Banerjee, J. Yan, D. G. Mandrus, S. E. Nagler, and N. P. Ong, "Oscillations of the thermal conductivity in the spin-liquid state of α-$RuCl_3$," Nat. Phys. **17**, 915 (2021).
[17]A. Kitaev, "Anyons in an exactly solved model and beyond," Ann. Phys. (NY) **321**, 2 (2006).
[18]X.-G. Zhou, H. Li, Y. H. Matsuda, A. Matsuo, W. Li, N. Kurita, K. Kindo, and H. Tanaka, "Intermediate quantum spin liquid phase in the Kitaev material α-$RuCl_3$ under high magnetic fields up to 100T," arXiv:2201.04597 (2022).
[19]S. Trebst and C. Hickey, "Kitaev materials," Phys. Rep. **950**, 1–37 (2022).
[20]X. Zhou, H. Li, J. Waugh, S. Parham, H.-S. Kim, J. Sears, A. Gomes, H.-Y. Kee, Y.-J. Kim, and D. Dessau, "Angle-resolved photoemission study of the Kitaev candidate α-$RuCl_3$," Phys. Rev. B **94**, 161106 (2016).
[21]S. Sinn, C. H. Kim, B. H. Kim, K. D. Lee, C. J. Won, J. S. Oh, M. Han, Y. J. Chang, N. Hur, H. Sato, B.-G. Park, C. Kim, H.-D. Kim, and T. W. Noh, "Electronic structure of the Kitaev material α-$RuCl_3$ probed by photoemission and inverse photoemission spectroscopies," Sci. Rep. **6**, 39544 (2016).
[22]S. Ghatak, A. N. Pal, and A. Ghosh, "Nature of electronic states in atomically thin MoS_2 field-effect transistors," ACS Nano **5**, 7707–7712 (2011).
[23]B. Shklovskii and A. Efros, *Electronic Properties of Doped Semiconductors* (Springer-Verlag, Berlin, 1984), pp. 228–244.
[24]H. Yi, B. Skinner, and B. I. Shklovskii, "Conductivity of two-dimensional small gap semiconductors and topological insulators in strong coulomb disorder," JETP **135**, 409–425 (2022).
[25]N. F. Mott, "Conduction in non-crystalline materials," Philosoph. Mag., A**19**, 835–852 (1969).
[26]D. J. Rizzo, B. S. Jessen, Z. Sun, F. L. Ruta, J. Zhang, J.-Q. Yan, L. Xian, A. S. McLeod, M. E. Berkowitz, K. Watanabe, T. Taniguchi, S. E. Nagler, D. G. Mandrus, A. Rubio, M. M. Fogler, A. J. Millis, J. C. Hone, C. R. Dean, and D. N. Basov, "Charge-transfer plasmon polaritons at graphene/α-$RuCl_3$ interfaces," Nano Lett. **20**, 8438–8445 (2020).
[27]B. Zhou, J. Balgley, P. Lampen-Kelley, J.-Q. Yan, D. G. Mandrus, and E. A. Henriksen, "Evidence for charge transfer and proximate magnetism in graphene–α-$RuCl_3$ heterostructures," Phys. Rev. B **100**, 165426 (2019).
[28]A. L. Efros and B. I. Shklovskii, "Coulomb gap and low temperature conductivity of disordered systems," J. Phys. C: Solid State Phys. **8**, L49 (1975).
[29]S. Reschke, F. Mayr, S. Widmann, H.-A. K. von Nidda, V. Tsurkan, M. V. Eremin, S.-H. Do, K.-Y. Choi, Z. Wang, and A. Loidl, "Sub-gap optical response in the Kitaev spin-liquid candidate α-$RuCl_3$," J. Phys.: Condens. Matter **30**, 475604 (2018).
[30]A. Ayari, E. Cobas, O. Ogundadegbe, and M. S. Fuhrer, "Realization and electrical characterization of ultrathin crystals of layered transition-metal dichalcogenides," J. Appl. Phys. **101**, 014507 (2007).
[31]R. Jayaraman and C. G. Sodini, "A 1/f noise technique to extract the oxide trap density near the conduction band edge of silicon," IEEE Trans. Electron Devices **36**, 1773–1782 (1989).
[32]J. Rodriguez, G. Lopez, F. Ramirez, N. P. Breznay, R. Kealhofer, V. Nagarajan, D. Latzke, S. Wilson, N. Marrufo, P. Santiago, J. Lara, A. Diego, E. Molina, D. Rosser, H. Tavassol, A. Lanzara, J. G. Analytis, and C. Ojeda-Aristizabal, "Competition between magnetic order and charge localization in Na_2IrO_3 thin crystal devices," Phys. Rev. B **101**, 235415 (2020).
[33]L. Moreschini, I. Lo Vecchio, N. P. Breznay, S. Moser, S. Ulstrup, R. Koch, J. Wirjo, C. Jozwiak, K. S. Kim, E. Rotenberg, A. Bostwick, J. G. Analytis, and A. Lanzara, "Quasiparticles and charge transfer at the two surfaces of the honeycomb iridate Na_2IrO_3," Phys. Rev. B **96**, 161116 (2017).
[34]S. Mashhadi, D. Weber, L. M. Schoop, A. Schulz, B. V. Lotsch, M. Burghard, and K. Kern, "Electrical transport signature of the magnetic fluctuation-structure relation in α-$RuCl_3$ nanoflakes," Nano Lett. **18**, 3203–3208 (2018).
[35]B. I. Shklovskii, "Hopping conduction in semiconductors subjected to a strong electric field," Sov. Phys. Semicond. **6**, 1964–1967 (1973).
[36]D. Yu, C. Wang, B. L. Wehrenberg, and P. Guyot-Sionnest, "Variable range hopping conduction in semiconductor nanocrystal solids," Phys. Rev. Lett. **92**, 216802 (2004).
[37]E. Levin and B. Shklovskii, "Low-temperature hopping conduction in strong electric fields. Numerical experiment a computer," Sov. Phys. Semicond. **18**, 534–539 (1984).
[38]I. I. Mazin, H. O. Jeschke, K. Foyevtsova, R. Valentí, and D. I. Khomskii, "Na_2IrO_3 as a molecular orbital crystal," Phys. Rev. Lett. **109**, 197201 (2012).
[39]K. Foyevtsova, H. O. Jeschke, I. I. Mazin, D. I. Khomskii, and R. Valentí, "*Ab initio* analysis of the tight-binding parameters and magnetic interactions in Na_2IrO_3," Phys. Rev. B **88**, 035107 (2013).
[40]Y. Li, K. Foyevtsova, H. O. Jeschke, and R. Valentí, "Analysis of the optical conductivity for A_2IrO_3 (A = Na, Li) from first principles," Phys. Rev. B **91**, 161101 (2015).